ADVANCED ELECTRONIC MATERIALS Open Access
www.advelectronicmat.de

Blends of Conjugated and Adhesive Polymers for Sticky Organic Thin-Film Transistors

*James G. Sutjianto, Sang H. Yoo, Clayton R. Westerman, Thomas N. Jackson, Jonathan J. Wilker, and Enrique D. Gomez**

Here, a polymer blend active layer that exhibits both electronic and adhesive properties is introduced. Various conjugated polymers are blended with a catechol-based polymer that shows high adhesion, such that blends serve as the active layer of multifunctional sticky organic thin-film transistors (OTFTs). Blend films maintain relatively constant field-effect charge carrier mobility in OTFTs regardless of composition. Lap shear adhesion strength tests show that all blend films exhibit adhesive properties with adhesion values ranging from 0.05 to 4.30 MPa. With relatively consistent mobility and the presence of adhesive properties at different compositions, blends of conjugated and adhesive polymers can lead to next-generation organic transistors for stable 3D stacking and waterproof adhesive sensors.

1. Introduction

Organic Thin-Film Transistors (OTFTs) have garnered substantial attention because of their large area compatibility,[1,2] potential solution processability,[3–5] and stretchability.[6,7] Previous efforts have fabricated OTFTs with field-effect charge carrier mobilities greater than 1 $cm^2\ V^{-1}\ s^{-1}$, which rivals commercially available hydrogenated amorphous silicon transistors.[8–11] Recently, it has been shown that blend systems can be utilized to achieve high-performance OTFTs.[12] Blends can be formulated to serve as the gate insulator layer[13,14] or the semiconductor active layer.[15,16] To serve as the active layer, blends of conjugated polymers,[17] conjugated polymers with insulating polymers,[18,19] and conjugated polymers with conjugated small molecules[20,21] have been demonstrated.

Conjugated polymers are amenable to blending, in particular when they are semicrystalline. Crystallization of the polymer creates a pure phase where charge conduction can occur unimpeded by secondary components.[22,23] The fibril-like crystallization motif of most conjugated polymers promotes the percolation of charge-conducting pathways.[24] The amorphous phase in conjugated polymers can uptake various other components without substantially disrupting conduction through crystalline domains. In addition, many of these polymers will often crystallize near an interface, thereby excluding other components and creating a conducting channel in bottom-gate bottom-contact transistors.[25]

One possible class of materials to blend with conjugated polymers includes adhesives. Strong adhesion is desirable to prevent delamination, especially under humid conditions, and to allow for 3D integration.[26,27] Previous work has developed polymers that mimic the adhesive protein that mussels use for strong underwater adhesion.[28] The amino acid 3,4-dihydroxyphenylalanine (DOPA), which is found in adhesive polypeptides, relies on several types of covalent and non-covalent bonds for strong adhesion to a variety of surfaces.[29] To mimic DOPA within adhesive proteins, 3,4-dihydroxystyrene can be distributed along a polymeric styrenic backbone, resulting in poly(catechol-styrene) (PCS).[30,31] These kinds of biomimetic polymers have significantly stronger underwater adhesion

J. G. Sutjianto, S. H. Yoo, E. D. Gomez
Department of Chemical Engineering
The Pennsylvania State University
University Park, PA 16802, USA
E-mail: edg12@psu.edu
C. R. Westerman, J. J. Wilker
Department of Chemistry
Purdue University
West Lafayette, IN 47907, USA
The ORCID identification number(s) for the author(s) of this article can be found under https://doi.org/10.1002/aelm.202300422

DOI: 10.1002/aelm.202300422

T. N. Jackson
Department of Electrical Engineering and Computer Science
The Pennsylvania State University
University Park, PA 16802, USA
T. N. Jackson, E. D. Gomez
Materials Research Institute
The Pennsylvania State University
University Park, PA 16802, USA
J. J. Wilker
School of Materials Engineering
Purdue University
West Lafayette, IN 47907, USA
E. D. Gomez
Department of Materials Science and Engineering
The Pennsylvania State University
University Park, PA 16802, USA

compared to commercial products.[29] Common epoxies have an underwater adhesion strength of ≈1 MPa, whereas biomimetic polymers, under optimized conditions, have a significantly stronger underwater adhesion strength of ≈3 MPa.[29] Because of their substantial underwater adhesion strength, they could enable a variety of bioelectronic applications.[32]

In this work, we blended PCS with three different kinds of conjugated polymers to fabricate OTFTs capable of strong adhesion. This approach introduces multifunctional thin-films that perform as semiconductors and exhibit "sticky" properties. Devices containing these polymer blends as the active layer have a modest drop off in mobility with the addition of the adhesive polymer, up to roughly half an order of magnitude. OTFTs fabricated using the novel polymer blend developed in this work present adhesion strength comparable to that of epoxy. Adhesion strength varies depending on the composition of the active layer; from 0.05 to 4.30 MPa based on PBTTT/PCS blends, from 0.29 to 4.29 MPa based on P3HT/PCS blends, and from 0.30 to 3.52 MPa based on PDPP/PCS blends. Thus, polymer blends involving PCS shown in this work can be used for stable vertical stacking of OTFTs in 3D architectures or be used in applications that require adhesion onto wet surfaces, such as in bioelectronics.

2. Results and Discussion

The conjugated polymers, adhesive polymer, and OTFT device architecture used in this study are shown in **Figure 1**. Two alkyl-thiophene derivatives, poly(3-hexylthiophene-2,5-diyl) (P3HT) and poly[2,5-bis(3-tetradecylthiophen-2-yl)thieno[3,2-b]thiophene] (PBTTT), along with a high-performance donor-acceptor polymer, poly[2,5-(2-octyldodecyl)−3,6-diketopyrrolopyrrole-alt-5,5-(2,5-di(thien-2-yl)thieno[3,2-b]thiophene)] (PDPP), were used to fabricate active layers of OTFTs. PCS was blended with conjugated polymers at various compositions and films were cast on bottom-gate bottom-contact substrates. The gate is heavily doped p-type silicon and the dielectric layer is 300 nm thermally grown silicon dioxide. Gold is used as both source and drain electrodes.

From the transfer curves of devices based on our blends (**Figure 2**a; Figures S1–S3, Supporting Information), threshold voltage for PBTTT/PCS devices shifts from −3.65 to 9.55 V, for P3HT/PCS devices the shift is from 5.97 to −1.32 V, and for PDPP/PCS devices threshold voltage increases from 9.52 to 18.9 V when PCS is added. Output curves of PBTTT/PCS blend (Figure S4, Supporting Information), P3HT/PCS blend (Figure S5, Supporting Information), and PDPP/PCS blend (Figure S6, Supporting Information) OTFTs have a linear regime and a saturation regime without a major sign of a contact resistance problem. In addition, pinch-off points occur at the correct drain voltage.

Mobility values were obtained in the region where mobility is roughly constant with gate voltage. Devices consisting of pure conjugated polymer have performance values similar to the ones reported in the literature.[33–36] Pure PCS films do not conduct charge, as expected (Figure S7, Supporting Information). Once the adhesive polymer is added, charge mobilities decrease by roughly half an order of magnitude when going from pristine conjugated polymer to either 25 or 20 wt.% conjugated polymer (Figure 2b; Figure S8, Supporting Information, for PBTTT/PCS blends; Figure S9, Supporting Information, for P3HT/PCS blends, and Figure S10, Supporting Information, for PDPP/PCS blends). For PBTTT/PCS blends, mobilities constantly decrease from 0.0742 to 0.0174 $cm^2\ V^{-1}\ s^{-1}$ when going from 100 wt.% PBTTT to 20 wt.% PBTTT. For P3HT/PCS blends, mobilities started at 0.0683 $cm^2\ V^{-1}\ s^{-1}$ for 100 wt.% P3HT and remain constant until 25 wt.% P3HT, where they decrease to 0.0421 $cm^2\ V^{-1}\ s^{-1}$. For PDPP/PCS blends, mobilities constantly decrease from 0.432 to 0.148 $cm^2\ V^{-1}\ s^{-1}$ when going from 100 wt.% PDPP to 20 wt.% PDPP. A decrease in mobility as the amount of insulative material increases is expected.[37,38] Although some decrease in charge mobility is observed, the decrease shown in Figure 2b is modest, such that blend films exhibit reasonable charge transport for a wide range of compositions.

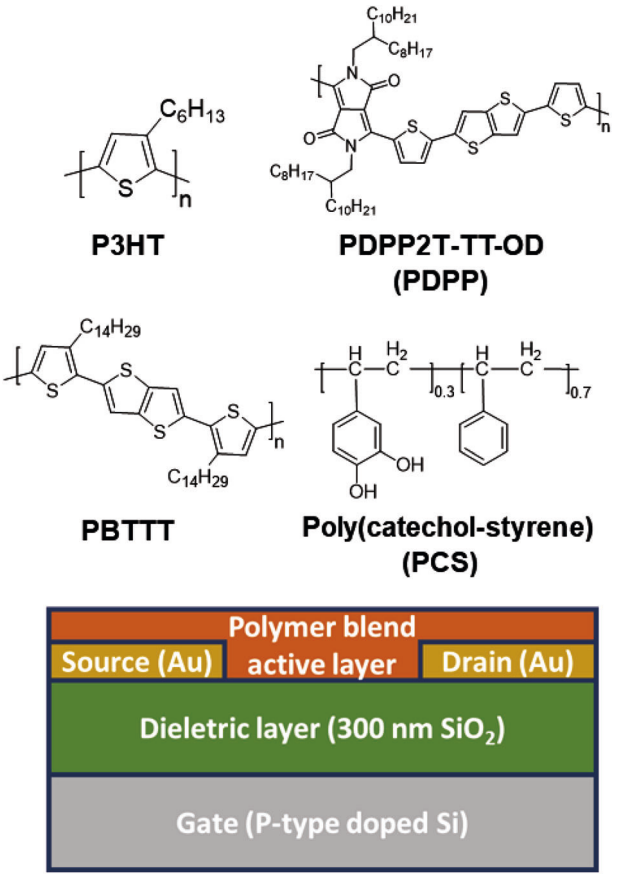

Figure 1. Chemical structures of polymers and schematic of OTFT device architecture used in this study.

Plots of mobility versus gate voltage for the three blend systems show that there are three different TFT behaviors occurring (Figure 2b; Figure S8, Supporting Information, for PBTTT/PCS blends; Figure S9, Supporting Information, for P3HT/PCS blends, and Figure S10, Supporting Information, for PDPP/PCS blends). For PBTTT/PCS blends, an eventual plateau of mobility at high gate voltage is indicative of a power-law mobility.[39] For P3HT/PCS blends, an increase then gradual decay in mobility represents a gradual decaying mobility.[39] For PDPP/PCS blends, the peak in the mobility

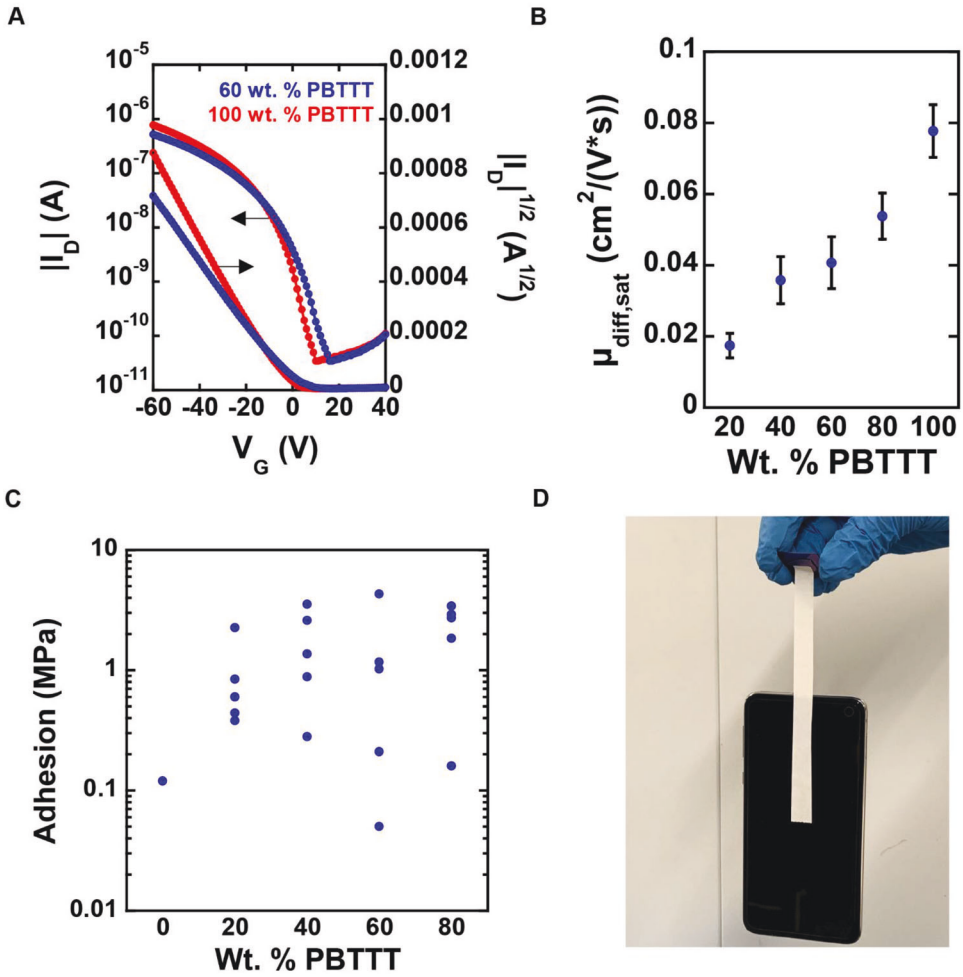

Figure 2. A) Transfer curves of devices with PBTTT as the active layer and PBTTT/PCS blend as the active layer with 60 wt.% PBTTT. B) Saturation mobility of devices with PBTTT/PCS blends as the active layer. The width and length of transistor channels are 220 and 320 µm, respectively. Error bars denote the standard deviation from measuring 10 devices per composition. C) Adhesion strength as a function of weight percent of PBTTT in the blended films. D) Image of bonded 60 wt.% PDPP films in between two silicon/silicon dioxide wafers holding a 156.3 g cellphone.

plot ("kink" in the transfer curve) is reminiscent of a transition from a contact-limited device at low gate voltages.[40] This device behavior is present in various previous studies of conjugated polymers with DPP moieties that are used as active layers in OTFTs.[41,42]

A lap shear strength test was used to quantitatively characterize the adhesive properties of blend films. PBTTT/PCS films can have adhesion from 0.05 to 4.30 MPa (Figure 2c), P3HT/PCS films can have adhesion from 0.29 to 4.23 MPa (Figure S11a, Supporting Information), and PDPP/PCS films can have adhesion from 0.30 to 3.52 MPa (Figure S12a, Supporting Information). The maximum adhesion for each conjugated polymer/PCS blend is about one-half of what is measured for cyanoacrylate superglue when bonding aluminum.[30] As an example of the adhesion strength of these blends, bonded 60 wt.% PDPP films (0.5 inch x 0.5 inch in bonding area and < 200 nm in thickness) can hold the weight of a 156.3 g cell phone, highlighting the strong adhesive bond (Figure 2d). In contrast, none of the neat conjugated polymers exhibit any adhesion. Overall, OTFTs with blends as the active layer possess good adhesive properties.

We used GIWAXS to reveal how blending PCS with conjugated polymers affects the crystallization of the conducting component. 2D data for PBTTT/PCS blends, P3HT/PCS blends, and PDPP/PCS blends are shown in Figures S13–S15 (Supporting Information), respectively. 1D scattering profiles are shown in **Figure 3** for PBTTT/PCS blends, Figure S16 (Supporting Information) for P3HT/PCS blends, and Figure S17 (Supporting Information) for PDPP/PCS blends. Intensities are normalized by exposure time, film thickness, and concentration of conjugated polymer. Azimuthally integrated (200) peak intensities in Figure S18 (Supporting Information) were used to determine the relative crystallinity of the active layers and are used to explain the trends observed in the device data. PBTTT/PCS blends (Figure S18a, Supporting Information) spectra show that the intensity of the (200) peak does not significantly change as PCS is added. For the P3HT/PCS blends (Figure S18b, Supporting Information), the spectra show that once PCS is added, the intensity of the (200) peak initially decreases and then retains similar intensities for larger amounts of PCS. GIWAXS data from PDPP/PCS blends (Figure S18c, Supporting Information) show a similar trend as

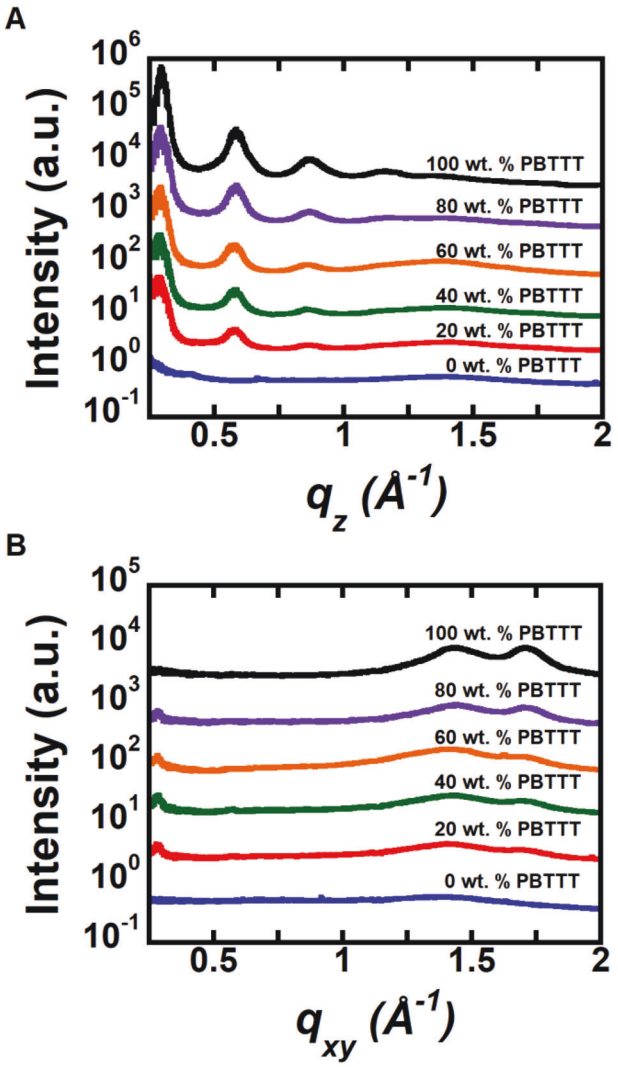

Figure 3. 1D GIWAXS A) out-of-plane profiles and B) in-plane profiles from PBTTT/PCS films. Data were normalized by exposure time, film thickness, and concentration of conjugated polymer.

data from PBTTT/PCS blends in that the intensity of the (200) peak does not significantly change as PCS is added.

Given the trends in GIWAXS data, we hypothesize that the up to 76.5% decrease in average mobility from 0.0742 to 0.0174 cm^2 V^{-1} s^{-1} as PCS is added to PBTTT is due to dilution of the conjugated polymer. In the case of P3HT/PCS devices, the trend in the relative degree of crystallinity of the active layer does not follow device average mobility results, e.g., 50 and 75 wt.% P3HT devices statistically have the same average mobility as pure P3HT devices. Retainment of the mobility with the addition of PCS is similar to previous results. Wang et al. have shown that the addition of regiorandom P3HT into a regioregular P3HT active layer does not lead to a decrease in charge mobility until regioregular P3HT content of the active layer is below 5.6 wt.%.[43] This is despite a drop in crystallinity and is a result of vertical phase separation, where regioregular P3HT crystallizes at the dielectric interface to form a conducting channel.[43] Likewise, P3HT/PCS blend devices have constant average mobility as low as 50 wt.% P3HT before a 38.4% decrease in average mobility from 0.0683 to 0.0421 cm^2 V^{-1} s^{-1} occurs at 25 wt.% P3HT even though crystallinity decreases once PCS is added. We hypothesize that similarly to the regioregular/regiorandom P3HT blend results, P3HT is present and prefers to crystallize at the semiconductor/dielectric layer interface even though PCS is present. For the PDPP/PCS system, an up to 65.7% decrease in average mobility from 0.432 to 0.148 cm^2 V^{-1} s^{-1} as PCS is added is likely due to dilution effects with the exception of the 60 wt.% PDPP and 80 wt.% PDPP blends. We suggest that lower average mobilities for those two systems are a consequence of the disruption of the conducting channel by the presence of PCS. The decrease in mobility in the PDPP/PCS devices could also be due to charge trapping by hydroxyl groups in PCS. Indeed, a less steep subthreshold slope from the transfer curves of PDPP/PCS blend devices is observed when compared to pristine PDPP devices, which could be a signature of induced traps. Nevertheless, we see no evidence of induced traps in the P3HT/PCS and PBTTT/PCS blends (no changes in subthreshold slope).

There are subtle changes in the alkyl spacing and π-π stacking distances once PCS is added. For PBTTT/PCS blends, the alkyl spacing distance increases from 21.5 up to 21.9 Å, and the π–π stacking distance increases from 3.69 up to 3.75 Å.[44,45] For P3HT/PCS blends, the alkyl spacing distance increases from 16.4 up to 16.6 Å, and the π–π stacking distance increases from 3.72 up to 3.75 Å.[46,47] For PDPP/PCS blends, the alkyl spacing distance increases from 19.6 Å up to 20.0 Å and the π–π stacking distance increases from 3.72 up to 3.77 Å.[48,49] In the PBTTT/PCS and P3HT/PCS systems, the addition of PCS causes some of the conjugated polymer chains to align in the face on orientation. For PBTTT/PCS blends, the in-plane alkyl spacing distance ranges from 22.0 to 22.8 Å, which is close to the out-of-plane alkyl spacing distance. For P3HT/PCS blends, the in-plane alkyl spacing distance ranges from 16.7 to 17.1 Å. An increase in alkyl spacing distance, π-π stacking distance, and the presence of in-plane alkyl spacing all are additional contributors to the decrease in field-effect charge carrier mobility as PCS is added.

Results from AFM, ToF-SIMS, and AR-XPS thin-film morphology characterization show how thin blend films can achieve good adhesion regardless of the composition of the active layer. AFM images of pristine PCS films show PCS on the surface as spheres or nodules (**Figure 4**a). Negative ion spectra of pristine PBTTT and PCS films from ToF-SIMS (Figure S19, Supporting Information) show that m/e of 135 is a good marker for PCS. The obtained images at m/e of 135 (Figure S20, Supporting Information) show that PCS appears as granular dots, thus confirming the dots that appear on the AFM images are PCS. We speculate that these spherical PCS particles act as adhesion sites for bonding to the film surface.

For PBTTT/PCS blend films, AFM images (Figure 4) show that RMS roughness decreases from 37.3 to 5.67 nm once PBTTT is added. The order of magnitude decrease in RMS roughness could cause stronger adhesion between the two films. The intensity of the S 2p signal of PBTTT at 30° (surface) is stronger than at 80° (bulk) in AR-XPS spectra. As such, AR-XPS spectra of PBTTT/PCS films (**Figure 5**; Figure S21, Supporting Information) suggest that PBTTT is rich at the surface of the film while PCS is rich in the bulk. In addition, the intensity of the O 1s signal of PCS either remains the same or gets stronger when the

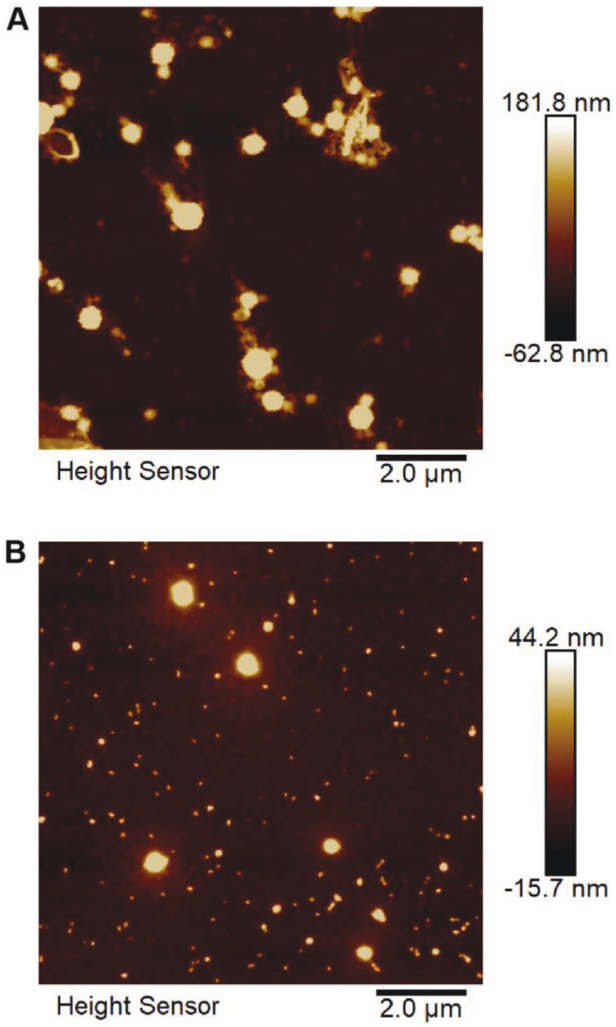

Figure 4. Atomic force microscopy height images of A) 0 wt.% PBTTT (RMS Roughness = 37.3 nm) and B) 80 wt.% PBTTT (RMS Roughness = 5.67 nm) films.

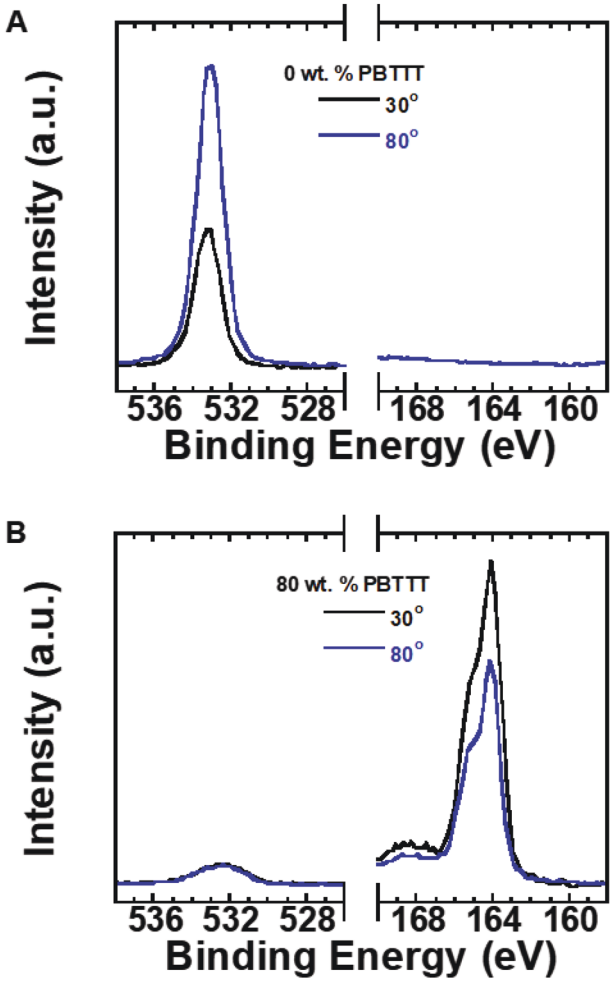

Figure 5. Angle-Resolved XPS measurements of A) 0 wt.% PBTTT and B) 80 wt.% PBTTT films at 30° and 80° takeoff angles. The signal on the left side of the plot (ca. 534 eV) represents the O 1s signal coming from PCS. The signal on the right side of the plot (ca. 164 eV) represents the S 2p signal coming from PBTTT.

takeoff angle changes from 30° (surface) to 80° (bulk). Although the S 2p signal is stronger on the surface, there is still sufficient PCS present on the surface to bond two films together.

The ability to bond all compositions of P3HT/PCS films can be explained using AFM and AR-XPS. 75 wt.% P3HT has the lowest RMS roughness compared to the other two blend compositions, 2.90 nm compared to as high as 44.3 nm (Figure S11b–e and Table S1, Supporting Information). AR-XPS shows the strongest O 1s signal at 25 wt.% P3HT when takeoff angle is 30° (Figure S22, Supporting Information). This suggests that PCS is rich in the surface at this composition compared to the other two blend compositions at 30° takeoff angle. The ability to bond all compositions of PDPP/PCS films can be explained in a similar manner as P3HT/PCS films. PCS is present on the surface of the films even though the surface is rich in PDPP (S 2p peak decreases as takeoff angles change from 30° to 80°) (Figure S23, Supporting Information). XPS data from blends of various compositions also confirms the enrichment of conjugated polymer at the surface of PBTTT/PCS films (Figure S24, Supporting Information). RMS roughness slightly increases as the amount of PDPP increases, from 43.8 nm at 20 wt.% PDPP to 47.4 nm at 60 wt.% PDPP. At 80 wt.% PDPP, due to the surface being significantly rich in PDPP, the RMS roughness decreases to 29.3 nm (Figure S12b–e and Table S2, Supporting Information). These characterization results indicate that a balance between surface roughness and the amount of PCS at the bonding interface plays an important role in the adhesion process, and that blending can be used to optimize thin-film adhesion by smoothening out the surface of the films and getting an adequate amount of PCS on the surface.

3. Conclusion

By creating blends of three different kinds of conjugated polymers along with PCS, multifunctional OTFTs that show both semiconductive and adhesive properties were fabricated. Different compositions of conjugated polymer and adhesive polymer in thin-films lead to a modest decrease in field-effect charge carrier mobilities, with the largest decrease being only roughly

half an order of magnitude for film compositions studied here (20–100 wt.% conjugated polymer). Adhesive properties of thin-films varied at each composition and different conjugated and adhesive polymer blends. The maximum adhesion strength for the blends was determined to be 4.30 MPa for PBTTT/PCS films. Various characterization techniques were used to explain the decrease in mobility and understand the thin-film morphology of the multifunctional active layer. A decrease in mobility can be attributed to dilution effects for PBTTT/PCS and PDPP/PCS blends, and a decrease in crystallinity for the P3HT/PCS blends as confirmed using GIWAXS. AFM images confirm a decrease in RMS roughness as the conjugated polymer is added to the active layer. The presence of PCS on the surface of the film as the conjugated polymer is added to the active layer is confirmed by AR-XPS. The successful blending of two unique polymers to fabricate multifunctional thin-films that exhibit both semiconducting and adhesive properties could enable OTFTs for bioelectronics and 3D integration applications.

4. Experimental Section

Materials: Poly(3-hexylthiophene-2,5-diyl) (P3HT) (EE97802, M_w = 36.6 kg mol^{-1}, Đ = 2.0) was purchased from Merck. Poly[2,5-bis(3-tetradecylthiophen-2-yl)thieno[3,2-b]thiophene] (PBTTT) (Product 753 971, M_w = 65.0 kg mol^{-1}, Đ = 2.5) was purchased from Millipore-Sigma. Poly[2,5-(2-octyldodecyl)−3,6-diketopyrrolopyrrole-alt-5,5-(2,5-di(thien-2-yl)thieno[3,2-b]thiophene)] (PDPP) (M0311A2, M_w = 204 kg mol^{-1}, Đ = 3.1) was purchased from Ossila. Poly[(3,4-dihydroxystyrene)-co-styrene] (M_w = 64.3 kg mol^{-1}, Đ = 2.3, Percent Catechol = 29.8%) was synthesized as previously described.[28,30,31] Anhydrous trichloroethylene, trichloro(octadecyl)silane (ODTS), anhydrous 1,2-Dichlorobenzene, and anhydrous 1,2,4-Trichlorobenzene were purchased from Millipore Sigma. Hexadecane was purchased from Alfa Aesar. Trimethoxy(octadecyl)silane (TMOS) was purchased from Acros Organics. Heavily doped p-type Si (100) wafers from Process Specialties were used for GIWAXS, AFM, and AR-XPS. Heavily doped p-type Si (100) wafers with a 300 nm thick thermally grown SiO_2 layer from Process Specialties were used for OTFTs, bonding samples, and ToF-SIMS.

OTFTs Fabrication and Testing: Solutions for OTFTs were prepared by dissolving the conjugated polymer and adhesive polymer in the corresponding solvent (1,2,4-Trichlorobenzene for P3HT/PCS, 1,2-Dichlorobenzene for PBTTT/PCS and PDPP/PCS) individually at a concentration of 10 mg mL^{-1} overnight on a 45 °C hotplate. Individual solutions were then distributed to get the correct weight percent blends. These blend solutions were then stirred on a 45 °C hotplate for ≈2 h. OTFT substrates consist of heavily doped p-type Si (100) wafers with a 300 nm thick thermally grown SiO_2 layer. 100 nm thick gold source and drain electrodes were evaporated onto the substrate and patterned using conventional double-layer lithography techniques at the Penn State Materials Research Institute Nanofabrication Laboratory. Substrates were cleaned with isopropanol and dried with dry air. They were then subjected to UV-Ozone for 20 min. After UV-Ozone, OTFT substrates were surface-treated with either 0.006 M TMOS in hexadecane (P3HT/PCS system) overnight at room temperature in air or 0.01 M ODTS in trichloroethylene (PBTTT/PCS & PDPP/PCS systems) for 20 min at room temperature in a nitrogen-filled glovebox. Substrates were then cleaned using isopropanol (P3HT/PCS system) or toluene and isopropanol (PBTTT/PCS and PDPP/PCS systems). TMOS-treated substrates were then dried with air. ODTS-treated substrates were dried with air and annealed at 120 °C for 20 min. Solutions were stirred at 90 °C prior to deposition. P3HT/PCS was spin-coated at 1000 RPM for 4 min after letting the deposited solution wet on the surface for 40 s. PBTTT/PCS was spin-coated at 2000 RPM for 2 min. PDPP/PCS was spin-coated at 1500 RPM for 2 min. Devices were then annealed at the following conditions. P3HT/PCS were annealed at 150°C for 3 h. PBTTT/PCS were annealed at 140 °C for 12.5 min. PDPP/PCS were annealed at 160 °C for 10 min. Devices were fabricated in bottom-gate and bottom-contact configurations. Devices were then tested using a Keithley 4200-SCS to obtain transfer curves in the saturation regime and output curves. Mobility equation (Equation (1)) in the saturation regime was used to extract hole mobility:

$$\mu_{\text{diff, sat}}\ (V_G) = \left(\frac{\partial\sqrt{I_D}}{\partial V_G}\right)^2 * \frac{2L}{W * C} \quad (1)$$

where I_D is the current between the source and drain electrodes, L and W are the length and width of the channel, $\mu_{\text{diff, sat}}$ is the differential charge mobility in the saturation regime, C is the capacitance of the dielectric, and V_G is the gate voltage. For all devices tested, L = 320 µm and W = 220 µm.

Lap Shear Strength Test: Lap shear strength test samples were prepared similarly to how OTFTs were fabricated. The only difference is that bare Si/SiO_2 was used. Two spin-coated samples were prepared for each bonding sample. Blend films were bonded with FM1202 Vacuum Mold Pressing Machine (Beijing Future Material Sci-Tech Co., Ltd.). One of the prepared samples was stacked on top of the other sample with both polymer film surfaces facing each other. One of the samples was made sure to be smaller than the other to ensure that the adjoining polymer surfaces overlap completely. Adjoined samples were then pressed at a constant pressure of 1 MPa and heated at 180 °C for 24 h for the curing process. After 24 h, the sample was allowed to cool for 6 h while still being pressed at a constant pressure of 1 MPa. The sample was then removed from the bonder. Bonded samples were then adhered to two ASTM acid-etched aluminum substrates using commercial epoxy. The substrates were drilled on one end for use in lap shear adhesion testing. Bonded silicon/silicon dioxide wafers were allowed to cure the aluminum for 24 h for maximum hold. Lap shear samples were tested using an Instron 5544 with a 2 kN load cell. The pull rate was set to 2 mm min^{-1} and allowed for complete failure of the bonded area.

Grazing-Incidence Wide-Angle X-Ray Scattering (GIWAXS): GIWAXS samples were cast on heavily doped p-type Si (100) wafers. Substrates were sonicated with acetone and isopropanol for 20 min each, dried with air, then subjected to UV-Ozone for 20 min. After UV-Ozone, surface treatment, spin coating thin-films, and annealing followed the same procedure as fabricating OTFTs. GIWAXS data were obtained on Beamline 7.3.3 at the Advanced Light Source, Lawrence Berkeley National Laboratory (λ = 1.24 Å) using 10 keV X-rays and a Pilatus detector. GIWAXS measurements were taken at an angle of incidence of 0.14°, which is above the critical angle of all materials. The obtained 2D data were reduced to 1D profiles using Xi-Cam.[50]

Atomic Force Microscopy (AFM): AFM samples were prepared similarly to how the GIWAXS samples were prepared. The samples were imaged with Bruker Dimension Icon Atomic Force Microscope using peak force tapping mode. The peak force set point was set at 1.5 nN.

Time-of-Flight Secondary Ion Mass Spectrometry (ToF-SIMS): ToF-SIMS samples were prepared similarly to how the OTFTs were fabricated. The only difference is that bare Si/SiO_2 was used. ToF-SIMS depth profiling was performed on a Physical Electronics NanoTOF II instrument. Samples were mounted behind a 5 mm aperture mask. The spectroscopy beam is 30 keV Bi_3^+ and the gas cluster ion beam (GCIB) is 5 keV Ar^+_{5000}. Spectroscopy beam raster size is 100 microns x 100 microns with a beam strength of ≈1.8 nA, 100 microns column aperture. GCIB raster size is 600 microns x 600 microns with a beam strength of 4.2 nA. The GCIB did 5 s etch per cycle for 30 cycles. Mass resolution is ≈3000 with contrast diaphragm out. The ratemeter is ≈25 kCPS during acquisition. For spectroscopy acquisition, 2 frames per cycle, 2 × 10^{10} dose, and 256 × 256 image resolution were used with an end mass of 1850. An Electron neutralizer was used for negative ion spectral acquisition. Electron and ion neutralization were used during GCIB sputtering.

Angle-Resolved X-Ray Photoelectron Spectroscopy (AR-XPS): AR-XPS samples were prepared similarly to how GIWAXS and AFM samples were

prepared. AR-XPS experiments were performed using a Physical Electronics VersaProbe II instrument equipped with a monochromatic Al kα X-ray source (h_v = 1486.7 eV) and a concentric hemispherical analyzer. Charge neutralization was performed using both low-energy electrons (<5 eV) and argon ions. The binding energy axis was calibrated using sputter-cleaned Cu (Cu $2p_{3/2}$ = 932.62 eV, Cu $3p_{3/2}$ = 75.1 eV) and Au foils (Au $4f_{7/2}$ = 83.96 eV).[51] Peaks were charge referenced to the CH_x band in the carbon 1s spectra at 284.8 eV. Measurements were made at takeoff angles of 30° and 80° with respect to the sample surface plane. This resulted in a typical sampling depth of 3–4 nm and 6–8 nm, respectively (95% of the signal originated from this depth or shallower). Quantification was done using instrumental relative sensitivity factors (RSFs) that account for the X-ray cross-section and inelastic mean free path of the electrons.

Supporting Information

Supporting Information is available from the Wiley Online Library or from the author.

Acknowledgements

J.G.S. and S.H.Y. contributed equally to this work. Financial support by the National Science Foundation under Award DMR-1921854 is acknowledged. J.G.S. acknowledges financial support from the National Science Foundation Graduate Research Fellowship Program (Award DGE-1255832). J.J.W. and C.R.W. appreciate the support provided by the Office of Naval Research (Award N00014-19-1-2342).

Conflict of Interest

The authors declare no conflict of interest.

Data Availability Statement

The data that support the findings of this study are available from the corresponding author upon reasonable request.

Keywords

adhesive films, conjugated polymers, organic thin-film transistors, polymer blends

Received: June 22, 2023
Revised: September 8, 2023
Published online: September 29, 2023

[1] M. Helgesen, J. E. Carlé, G. A. Dos Reis Benatto, R. R. Søndergaard, M. Jørgensen, E. Bundgaard, F. C. Krebs, *Adv. Energy Mater.* **2015**, *5*, 1401996.
[2] D. Khim, G.-S. Ryu, W.-T. Park, H. Kim, M. Lee, Y.-Y. Noh, *Adv. Mater.* **2016**, *28*, 2752.
[3] B. H. Smith, M. B. Clark, H. Kuang, C. Grieco, A. V. Larsen, C. Zhu, C. Wang, A. Hexemer, J. B. Asbury, M. J. Janik, E. D. Gomez, *Adv. Funct. Mater.* **2015**, *25*, 542.
[4] B. H. Smith, Q. Zhang, M. A. Kelly, J. H. Litofsky, D. Kumar, A. Hexemer, W. You, E. D. Gomez, *ACS Macro Lett.* **2017**, *6*, 1162.
[5] K. Vakhshouri, B. H. Smith, E. P. Chan, C. Wang, A. Salleo, C. Wang, A. Hexemer, E. D. Gomez, *Macromolecules* **2016**, *49*, 7359.
[6] A. X. Chen, A. T. Kleinschmidt, K. Choudhary, D. J. Lipomi, *Chem. Mater.* **2020**, *32*, 7582.
[7] Y. Zheng, G.-J. N. Wang, J. Kang, M. Nikolka, H.-C. Wu, H. Tran, S. Zhang, H. Yan, H. Chen, P. Y. Yuen, J. Mun, R. H. Dauskardt, I. Mcculloch, J. B.-H. Tok, X. Gu, Z. Bao, *Adv. Funct. Mater.* **2019**, *29*, 1905340.
[8] Y. Yamashita, F. Hinkel, T. Marszalek, W. Zajaczkowski, W. Pisula, M. Baumgarten, H. Matsui, K. Müllen, J. Takeya, *Chem. Mater.* **2016**, *28*, 420.
[9] Y. Yuan, G. Giri, A. L. Ayzner, A. P. Zoombelt, S. C. B. Mannsfeld, J. Chen, D. Nordlund, M. F. Toney, J. Huang, Z. Bao, *Nat. Commun.* **2014**, *5*, 3005.
[10] W. Zhang, Y. Han, X. Zhu, Z. Fei, Y. Feng, N. D. Treat, H. Faber, N. Stingelin, I. Mcculloch, T. D. Anthopoulos, M. Heeney, *Adv. Mater.* **2016**, *28*, 3922.
[11] A. F. Paterson, L. Tsetseris, R. Li, A. Basu, H. Faber, A.-H. Emwas, J. Panidi, Z. Fei, M. R. Niazi, D. H. Anjum, M. Heeney, T. D. Anthopoulos, *Adv. Mater.* **2019**, *31*, 1900871.
[12] Y. Pan, G. Yu, *Chem. Mater.* **2021**, *33*, 2229.
[13] D. Thuau, K. Kallitsis, S. Ha, F. Bargain, T. Soulestin, G. Pecastaings, S. Tenc-Girault, F. D. Dos Santos, G. Hadziioannou, *Adv. Electron. Mater.* **2020**, *6*, 1901250.
[14] D. Khim, Y. Xu, K.-J. Baeg, M. Kang, W.-T. Park, S.-H. Lee, I.-B. Kim, J. Kim, D.-Y. Kim, C. Liu, Y.-Y. Noh, *Adv. Mater.* **2016**, *28*, 518.
[15] M. J. Han, M. Mcbride, B. Risteen, G. Zhang, B. V. Khau, E. Reichmanis, D. K. Yoon, *Chem. Mater.* **2020**, *32*, 688.
[16] Y. Lei, P. Deng, Q. Zhang, Z. Xiong, Q. Li, J. Mai, X. Lu, X. Zhu, B. S. Ong, *Adv. Funct. Mater.* **2018**, *28*, 1706372.
[17] J. I. Scott, X. Xue, M. Wang, R. J. Kline, B. C. Hoffman, D. Dougherty, C. Zhou, G. Bazan, B. T. O'connor, *ACS Appl. Mater. Interfaces* **2016**, *8*, 14037.
[18] S. Goffri, C. Müller, N. Stingelin-Stutzmann, D. W. Breiby, C. P. Radano, J. W. Andreasen, R. Thompson, R. A. J. Janssen, M. M. Nielsen, P. Smith, H. Sirringhaus, *Nat. Mater.* **2006**, *5*, 950.
[19] I. Angunawela, M. M. Nahid, M. Ghasemi, A. Amassian, H. Ade, A. Gadisa, *ACS Appl. Mater. Interfaces* **2020**, *12*, 26239.
[20] J. Smith, W. Zhang, R. Sougrat, K. Zhao, R. Li, D. Cha, A. Amassian, M. Heeney, I. Mcculloch, T. D. Anthopoulos, *Adv. Mater.* **2012**, *24*, 2441.
[21] J. Chen, M. Shao, K. Xiao, Z. He, D. Li, B. S. Lokitz, D. K. Hensley, S. M. Kilbey, J. E. Anthony, J. K. Keum, A. J. Rondinone, W.-Y. Lee, S. Hong, Z. Bao, *Chem. Mater.* **2013**, *25*, 4378.
[22] D. R. Kozub, K. Vakhshouri, L. M. Orme, C. Wang, A. Hexemer, E. D. Gomez, *Macromolecules* **2011**, *44*, 5722.
[23] A. T. Hidayat, H. Benten, N. Ohta, Y. Na, A. Muraoka, H. Kojima, M.-C. Jung, M. Nakamura, *Macromolecules* **2020**, *53*, 6630.
[24] S. A. Mollinger, B. A. Krajina, R. Noriega, A. Salleo, A. J. Spakowitz, *ACS Macro Lett.* **2015**, *4*, 708.
[25] W. Zhang, E. D. Gomez, S. T. Milner, *Macromolecules* **2016**, *49*, 963.
[26] Y. G. Seol, N.-E. Lee, S. H. Park, J. Y. Bae, *Org. Electron.* **2008**, *9*, 413.
[27] T. S. Glen, N. W. Scarratt, H. Yi, A. Iraqi, T. Wang, J. Kingsley, A. R. Buckley, D. G. Lidzey, A. M. Donald, *J. Polym. Sci. B: Polym. Phys* **2016**, *54*, 216.
[28] G. Westwood, T. N. Horton, J. J. Wilker, *Macromolecules* **2007**, *40*, 3960.
[29] M. A. North, C. A. Del Grosso, J. J. Wilker, *ACS Appl. Mater. Interfaces* **2017**, *9*, 7866.
[30] C. R. Matos-Pérez, J. D. White, J. J. Wilker, *J. Am. Chem. Soc.* **2012**, *134*, 9498.
[31] H. J. Meredith, C. L. Jenkins, J. J. Wilker, *Adv. Funct. Mater.* **2014**, *24*, 3259.
[32] C. Xie, X. Wang, H. He, Y. Ding, X. Lu, *Adv. Funct. Mater.* **2020**, *30*, 1909954.

[33] P. Boufflet, Y. Han, Z. Fei, N. D. Treat, R. Li, D.-M. Smilgies, N. Stingelin, T. D. Anthopoulos, M. Heeney, *Adv. Funct. Mater.* **2015**, *25*, 7038.
[34] I. Mcculloch, M. Heeney, C. Bailey, K. Genevicius, I. Macdonald, M. Shkunov, D. Sparrowe, S. Tierney, R. Wagner, W. Zhang, M. L. Chabinyc, R. J. Kline, M. D. Mcgehee, M. F. Toney, *Nat. Mater.* **2006**, *5*, 328.
[35] J.-F. Chang, B. Sun, D. W. Breiby, M. M. Nielsen, T. I. Sölling, M. Giles, I. Mcculloch, H. Sirringhaus, *Chem. Mater.* **2004**, *16*, 4772.
[36] Y. Li, S. P. Singh, P. Sonar, *Adv. Mater.* **2010**, *22*, 4862.
[37] H. Tran, V. R. Feig, K. Liu, H.-C. Wu, R. Chen, J. Xu, K. Deisseroth, Z. Bao, *ACS Cent. Sci.* **2019**, *5*, 1884.
[38] C.-C. Lin, S. N. Afraj, A. Velusamy, P.-C. Yu, C.-H. Cho, J. Chen, Y.-H. Li, G.-H. Lee, S.-H. Tung, C.-L. Liu, M.-C. Chen, A. Facchetti, *ACS Nano* **2021**, *15*, 727.
[39] C. Liu, G. Li, R. Di Pietro, J. Huang, Y.-Y. Noh, X. Liu, T. Minari, *Phys. Rev. Appl.* **2017**, *8*, 034020.
[40] E. G. Bittle, J. I. Basham, T. N. Jackson, O. D. Jurchescu, D. J. Gundlach, *Nat. Commun.* **2016**, *7*, 10908.
[41] P. Sonar, J. Chang, Z. Shi, E. Gann, J. Li, J. Wu, C. R. Mcneill, *J. Mater. Chem. C* **2015**, *3*, 9299.
[42] J. Li, Y. Zhao, H. S. Tan, Y. Guo, C.-A. Di, G. Yu, Y. Liu, M. Lin, S. H. Lim, Y. Zhou, H. Su, B. S. Ong, *Sci. Rep.* **2012**, *2*, 754.
[43] C. Wang, J. Rivnay, S. Himmelberger, K. Vakhshouri, M. F. Toney, E. D. Gomez, A. Salleo, *ACS Appl. Mater. Interfaces* **2013**, *5*, 2342.
[44] J. E. Cochran, M. J. N. Junk, A. M. Glaudell, P. L. Miller, J. S. Cowart, M. F. Toney, C. J. Hawker, B. F. Chmelka, M. L. Chabinyc, *Macromolecules* **2014**, *47*, 6836.
[45] N. Kamatham, O. A. Ibraikulov, P. Durand, J. Wang, O. Boyron, B. Heinrich, T. Heiser, P. Lévêque, N. Leclerc, S. Méry, *Adv. Funct. Mater.* **2021**, *31*, 2007734.
[46] P.-H. Chu, G. Wang, B. Fu, D. Choi, J. O. Park, M. Srinivasarao, E. Reichmanis, *Adv. Electron. Mater.* **2016**, *2*, 1500384.
[47] C. Zhai, X. Yang, S. Han, G. Lu, P. Wei, A. Chumakov, E. Erbes, Q. Chen, S. Techert, S. V. Roth, P. Zhang, L. Bu, *Chem. Mater.* **2021**, *33*, 2673.
[48] N. Wu, G. Huang, H. Huang, Y. Wang, X. Gu, X. Wang, L. Qiu, *Macromol. Rapid Commun.* **2023**, *44*, 2300169.
[49] Z. Wu, Y. Wu, J. Yang, Y. Yan, W. Li, L. Yang, Q. Chen, Z. Yi, Y. Liu, S. Chen, Y. Zhao, *Adv. Electron. Mater.* **2023**, *9*, 2300029.
[50] R. J. Pandolfi, D. B. Allan, E. Arenholz, L. Barroso-Luque, S. I. Campbell, T. A. Caswell, A. Blair, F. De Carlo, S. Fackler, A. P. Fournier, G. Freychet, M. Fukuto, D. Gürsoy, Z. Jiang, H. Krishnan, D. Kumar, R. J. Kline, R. Li, C. Liman, S. Marchesini, A. Mehta, A. T. N'diaye, D. Y. Parkinson, H. Parks, L. A. Pellouchoud, T. Perciano, F. Ren, S. Sahoo, J. Strzalka, D. Sunday, et al., *J. Synchrotron. Radiat.* **2018**, *25*, 1261.
[51] M. P. Seah, *Surf. Interface Anal.* **2001**, *31*, 721.